nanomaterials

MDPI

Article

Polymer-Assisted Synthesis of Co_3O_4 Spinel Catalysts with Enhanced Surface Co^{2+} Ions for N_2O Decomposition

Nahea Kim [1,2], Su-Jin Kim [1], Sang-Hyeok Seo [1], Myeung-Jin Lee [1], Bora Jeong [1], Hong-Dae Kim [1], Tae Won Nam [2,*] and Bora Ye [1,*]

[1] Ulsan Technology Application Division, Korea Institute of Industrial Technology, Ulsan 44413, Republic of Korea; nahea007@kitech.re.kr (N.K.); sujini@kitech.re.kr (S.-J.K.); seosang0422@kitech.re.kr (S.-H.S.); leemj@kitech.re.kr (M.-J.L.)

[2] Department of Materials Science and Engineering, Pusan National University, Busan 46241, Republic of Korea

* Correspondence: namtaewon@pusan.ac.kr (T.W.N.); yebora@kitech.re.kr (B.Y.); Tel.: +82-51-510-2445 (T.W.N.); +82-52-980-6644 (B.Y.); Fax: +82-52-980-6644 (B.Y.)

Abstract

Nitrous oxide (N_2O) is a potent greenhouse gas with a global warming potential > 310 times that of CO_2. Owing to its rapid increase in atmospheric concentrations from industrial emissions, N_2O poses increasing environmental concerns. Among the various N_2O abatement technologies, catalytic decomposition can directly convert N_2O into harmless N_2 and O_2 without generating secondary pollutants. In this study, Co_3O_4 spinel catalysts were synthesized using a polymer-assisted precipitation method, using polyvinyl alcohol, polyvinylpyrrolidone, or polyethylene glycol (PEG) as N_2O decomposition catalysts. The PEG-mediated synthesis method yielded the most active catalyst with superior N_2O decomposition efficiency. Structural and surface analyses confirmed that PEG facilitated the formation of Co^{2+}-enriched surface sites and abundant oxygen vacancies, which are crucial active sites for N_2O adsorption and activation. Moreover, these features improved the redox properties and electron transfer behavior of the resulting catalyst. In particular, the PEG-derived $5Co_3O_4/CeO_2$ catalyst exhibited enhanced N_2O decomposition activity and stability even in the presence of coexisting N_2O and O_2, highlighting its potential for real-world applications. This study provides an effective synthetic route for Co_3O_4-based catalysts and potential opportunities for wide applications in industrial N_2O removal.

Keywords: Nitrous oxide decomposition; Co_3O_4 spinel catalyst; surface Co^{2+} species

check for updates

Academic Editor: Hangrong Chen

Received: 16 September 2025
Revised: 21 October 2025
Accepted: 23 October 2025
Published: 28 October 2025

Citation: Kim, N.; Kim, S.-J.; Seo, S.-H.; Lee, M.-J.; Jeong, B.; Kim, H.-D.; Nam, T.W.; Ye, B. Polymer-Assisted Synthesis of Co_3O_4 Spinel Catalysts with Enhanced Surface Co^{2+} Ions for N_2O Decomposition. *Nanomaterials* **2025**, *15*, 1642. https://doi.org/10.3390/nano15211642

Copyright: © 2025 by the authors. Licensee MDPI, Basel, Switzerland. This article is an open access article distributed under the terms and conditions of the Creative Commons Attribution (CC BY) license (https://creativecommons.org/licenses/by/4.0/).

1. Introduction

Nitrous oxide (N_2O) has recently surpassed chlorofluorocarbons (CFCs) as the predominant anthropogenic ozone-depleting substance and is the third most significant greenhouse gas following CO_2 and CH_4 [1–3]. Although N_2O represents a relatively small fraction of total greenhouse gas emissions, its global warming potential is approximately 310 times higher than that of CO_2, and its ozone depletion potential is nearly double that of CFCs [4,5]. The continuous increase in atmospheric N_2O concentrations caused by industrial activities, including nitric and adipic acid production, semiconductor manufacturing, fossil fuel combustion, co-firing power generation, and maritime emissions, has become an increasingly serious environmental concern [6–8]. N_2O emissions are expected to double by 2050, rendering the development and implementation of effective reduction strategies urgently required. Various mitigation strategies have been developed, including thermal decomposition and catalytic reduction [9,10]. Among them, the direct catalytic decomposition of N_2O into

harmless N_2 and O_2 is a promising approach owing to the absence of secondary pollutants and its simplicity and high efficiency [11,12]. For the direct catalytic decomposition of N_2O, extensive research has focused on three primary catalyst categories: supported noble metals [13–15], pure and composite metal oxides [11,16–18], and zeolite-based systems [19–21]. Among these, metal oxide catalysts with excellent thermal stability at high temperatures are being researched as an alternative to overcome disadvantages such as the high cost of noble metal catalysts, low hydrothermal stability, and catalyst activity degradation by other gas components of zeolite catalysts [22,23]. In particular, spinel-type Co_3O_4 (AB_2O_4), in which Co^{2+} occupies tetrahedral (A) sites and Co^{3+} occupies octahedral (B) sites, has been widely investigated for N_2O decomposition. Spinel-type Co_3O_4 possesses the favorable redox properties of Co^{2+} and the high density of oxygen vacancies [24,25]. Although Co_3O_4-based catalysts offer advantages for N_2O decomposition, they often exhibit reduced activity in the presence of interfering gases, such as O_2. These interfering gases compete with N_2O for active sites and hinder the reaction by suppressing the role of surface oxygen vacancies [26,27]. While several synthesis strategies, such as doping and defect engineering, have been explored for tuning the Co^{3+}/Co^{2+} ratio, these methods often entail complex procedures or harsh, high-temperature post-treatments [28,29]. In contrast, the polymer-assisted synthesis offers a facile, energy-efficient, and cost-effective route to concurrently modulate the surface electronic structure and active sites [30]. This is achieved through the coordination between polymer functional groups (e.g., PVA, PVP, PEG) and cobalt precursors, which enables the precise control of the Co^{3+}/Co^{2+} ratio and oxygen-vacancy formation under mild reaction conditions, without requiring additional doping or post-treatment [31,32].

To address these limitations, polyvinyl alcohol (PVA), polyvinylpyrrolidone (PVP), and polyethylene glycol (PEG) have been employed as polymeric additives owing to their distinct physicochemical properties. For example, PVA exhibits mild reducing properties [33,34], and PVP stabilizes particle dispersion [34,35]. PEG provides strong coordination capability and promotes the formation of surface-active sites and oxygen vacancies. In particular, PEG has emerged as an effective modifier, achieving the highest N_2O conversion owing to its abundant hydroxyl groups and flexible molecular backbone, which facilitate enhanced interactions with metal precursors [36–38]. Recent density functional theory calculations have demonstrated that the polymer-induced electronic modulation of the surface cobalt oxidation states, coupled with the generation of oxygen vacancies, can effectively decrease the activation energy for N_2O decomposition [39,40]. Although polymer-assisted synthesis is generally used for morphological control or particle stabilization, its potential role in modulating the surface electronic properties, particularly in oxidative environments, has not been extensively investigated.

In this study, PVA, PVP, and PEG were employed as polymeric additives to modulate the surface properties and electronic structures of Co_3O_4 catalysts. To evaluate their catalytic performance, Co_3O_4 catalysts, which were synthesized using polymer additives, were supported on CeO_2 to form $5Co_3O_4/CeO_2$ composite catalysts. CeO_2 was selected because it is widely known for its high oxygen storage capacity and strong redox ability, which promote the formation of surface oxygen vacancies and enhance oxygen mobility [36]. By varying the polymer additives used during synthesis, the Co^{2+}/Co^{3+} ratio was successfully tuned and abundant surface oxygen vacancies were introduced, enhancing the N_2O decomposition activity. The polymer-assisted strategy enabled the formation of Co_3O_4 surfaces rich in Co^{2+} and oxygen vacancies, achieving enhanced catalytic activity even under high gas hourly space velocity (GHSV) conditions. Notably, the optimized PEG catalyst maintained over 98% N_2O conversion above 550 °C even under oxygen-rich conditions, further indicating its potential applicability in realistic industrial environments.

2. Materials and Methods

2.1. Materials

Cobalt(II) nitrate hexahydrate ($Co(NO_3)_2 \cdot 6H_2O$) and cerium(IV) oxide (CeO_2) were purchased from Sigma-Aldrich (St. Louis, MO, USA). PVA [$CH_2CH(OH)n$], PVP [$(C_6H_9NO)n$], PEG [$H((CH_2CH_2O)n)OH$], and sodium hydroxide (NaOH) were obtained from Daejung Chemicals and Metals Co., Ltd. (Siheung-si, Gyeonggi-do, Republic of Korea).

2.2. Preparation of Polymer-Assisted Co_3O_4 Spinel Catalysts Using PVA, PVP, and PEG

Polymer-assisted Co_3O_4 spinel catalysts were synthesized using a precipitation method. Briefly, 1.0 and 10.0 g of polymer and NaOH, respectively, were dissolved in 100 mL of deionized (DI) water and stirred for 1 h. Subsequently, 15.0 g of $Co(NO_3)_2 \cdot 6H_2O$ was dissolved in 100 mL of DI water and stirred for 1 h. A mixed solution of the polymer and NaOH was slowly added dropwise to the prepared cobalt solution. The pink precipitate formed from the initial blue solution was washed with ethanol and DI water and repeatedly centrifuged until the pH became neutral. Subsequently, the catalyst precursors were dried at 100 °C for 6 h in an oven and calcined at 650 °C for 4 h in a muffle furnace. The synthesized PEG-, PVP-, and PVA-based catalysts were labeled as PEG Co_3O_4, PVP Co_3O_4, and PVA Co_3O_4, respectively.

2.3. Synthesis of Polymer-Assisted Co_3O_4/CeO_2 Catalysts

Using the impregnation method, the polymer-assisted (PVA, PVP, or PEG) catalysts were used as precursors to obtain CeO_2-supported catalysts ($5Co_3O_4/CeO_2$). Briefly, 5 wt% polymer-assisted (PVA, PVP, or PEG) Co_3O_4 was stirred in 100 mL of DI water for 30 min, while CeO_2 was stirred in 150 mL of DI water for 30 min. The solutions were mixed together and stirred for 1 h. The catalysts were dried at 100 °C for 6 h in an oven and calcined at 650 °C for 4 h in a muffle furnace. The PEG-, PVP-, and PVA-assisted/CeO_2-supported catalysts were labeled as PEG $5Co_3O_4/CeO_2$, PVP $5Co_3O_4/CeO_2$, and PVA $5Co_3O_4/CeO_2$, respectively. To enhance visual clarity and comprehensibility, the overall synthesis route has been illustrated as a schematic representation, which has been incorporated into the Figure S1.

2.4. Catalyst Characterization

The structural characteristics of the catalysts were analyzed using X-Ray diffraction (XRD; D8 Advance, Bruker, Billerica, MA, USA) with Cu Kα radiation over a 2θ range of 10–80° to confirm the formation of the spinel Co_3O_4 phase and to evaluate the effect of polymer additives on crystallinity. The morphology and lattice structure of the catalysts were examined using field emission transmission electron microscopy (JEM-F200, JEOL, Ltd., Tokyo, Japan) operated at 200 kV. The specific surface areas and pore volumes of the catalysts were determined using the Brunauer–Emmett–Teller (BET) and Barrett–Joyner–Halenda methods with an ASAP 2020 instrument (Micromeritics, Norcross, GA, USA) to assess the influence of polymer-assisted synthesis on textural properties. Prior to obtaining measurements, the samples were pretreated at 150 °C for 4 h under vacuum with N_2 gas to remove impurities and moisture. Bonding between the polymer and metal ion state (Co^{2+} and Co^{3+}) was evaluated using Fourier-transform infrared (FT-IR) spectroscopy (Vertex 80v, Bruker, USA). The presence of residual polymer was confirmed using a micro-Raman spectrometer (NRS-5100, JASCO, Tokyo, Japan) with a laser wavelength of 532 nm. X-Ray photoelectron spectroscopy (XPS; K-Alpha, Thermo Fisher Scientific, Waltham, MA, USA) using an Al Kα radiation source (λ = 1.4866 Å) was conducted to investigate the chemical states of elements in the polymer-assisted Co_3O_4/CeO_2 catalyst. The XPS binding energy was calibrated using the C 1s peak at 284.6 eV. Electron paramagnetic resonance (EPR)

spectroscopy (Bruker, Billerica, MA, USA, EMXplus) was performed at X-band ~9.518 GHz with a magnetic field 1500 G to measure the unpaired electron signals of Co^{2+} ions for identification and quantification. Temperature-programmed reduction with H_2 (H_2-TPR) and temperature-programmed desorption with O_2 (O_2-TPD) and N_2O (N_2O-TPD) were performed to evaluate the redox behavior, oxygen mobility, using a chemisorption analyzer (AutoChem II 2920, Micromeritics, USA) by increasing the temperature from 100 to 700 °C at a rate of 10 °C/min.

2.5. Catalytic Performance Evaluation

The N_2O decomposition activity was evaluated at 350–650 °C using a fixed-bed reactor with a reactor diameter and length of 12.7 and 400 mm, respectively. The feed-gas flow rate was regulated using a mass-flow controller (Brooks Instruments, Hatfield, PA, USA). The total flow rate of the feed gas was maintained at 500 sccm. For each test, 0.9 g of catalyst was loaded onto quartz wool 0.3 g to prevent channeling and maintain a stable fixed-bed configuration during the reaction. The evaluation gas flow conditions were as follows: 5000 ppm of N_2O, 5 vol% O_2 (when used), balanced N_2, and GHSV of 60,000 h^{-1}. FT-IR spectroscopy (CX-4000, Gasmet Technologies Oy, Helsinki, Finland) was employed to analyze the inlet and outlet reaction gas concentrations (except O_2), while the O_2 concentration was measured using a gas analysis spectrometer (DSM-XT, Hausnet S.R.L., Buenos Aires, Argentina). The N_2O conversion efficiency was calculated using Equation (1), where $[N_2O]_{in}$ and $[N_2O]_{out}$ represent the N_2O concentrations (ppm) in the feed and flue gases, respectively.

$$N_2O\ conversion\ (\%) = \frac{[N_2O]_{in} - [N_2O]_{out}}{[N_2O]_{in}} \times 100 \quad (1)$$

3. Results & Discussion

3.1. Catalytic Performance

The catalytic activity of the synthesized polymer-assisted $5Co_3O_4/CeO_2$ catalysts was evaluated for N_2O decomposition using a fixed-bed reactor. As shown in Figure 1a, all polymer-assisted catalysts exhibited enhanced N_2O conversion compared to the pristine Co_3O_4/CeO_2. Among them, PEG $5Co_3O_4/CeO_2$ demonstrated the highest activity, achieving >99.5% conversion at 600 °C. In contrast, the pristine sample reached a maximum conversion of 57.6% under identical conditions. This trend highlights the promotional effect of polymer-induced surface modification, particularly by PEG, on catalytic performance for N_2O decomposition. The catalytic activity trend observed in Figure S2 for polymer-assisted Co_3O_4 catalysts was consistent with that of the corresponding $5Co_3O_4/CeO_2$ catalysts. To ensure that the intrinsic catalytic activity was accurately evaluated and to eliminate surface area effects as shown in Figure S3, the N_2O decomposition reaction was performed under kinetically controlled conditions, where mass-transfer limitations were excluded according to the Koros–Nowak criterion [41,42]. All catalytic measurements were carried out at a GHSV 1,000,000 h^{-1}, while maintaining the N_2O conversion below 20%, consistent with previously reported kinetic control conditions [43]. The apparent activation energies (E_a) for the Co_3O_4 catalysts were determined to be 73.94 kJ·mol^{-1} for pristine Co_3O_4, 59.42 kJ·mol^{-1} for PVA Co_3O_4, kJ·mol^{-1} for PVP Co_3O_4, and kJ·mol^{-1} for PEG Co_3O_4. Significantly, PEG Co_3O_4 exhibited the lowest E_a, indicating that the polymer-assisted precipitation strategy effectively increased the density of accessible active sites and enhanced surface reducibility, thereby improving the intrinsic catalytic activity toward N_2O decomposition.

To investigate the effect of O_2 on N_2O decomposition owing to competitive adsorption on the catalyst surface, catalytic activity under O_2 co-feeding conditions was evaluated for the best-performing (PEG $5Co_3O_4/CeO_2$) and least active (pristine $5Co_3O_4/CeO_2$)

catalysts [31,44]. As shown in Figure 1b, the presence of 5 vol% O_2 suppressed N_2O conversion across all temperatures. The observed inhibitory effect is consistent with previous studies, which have reported that the coexistence of O_2 suppresses N_2O decomposition due to competitive adsorption on the active sites of Co_3O_4-based catalysts [45–48]. However, PEG $5Co_3O_4/CeO_2$ retained high activity even in the presence of O_2, reaching 97.6% conversion at 600 °C. In contrast, the pristine $5Co_3O_4/CeO_2$ catalyst showed significantly reduced performance, with a maximum conversion decreasing to 35.4% under identical conditions. Thus, PEG $5Co_3O_4/CeO_2$ exhibited enhanced intrinsic activity and superior resistance to oxygen-induced inhibition. Long-term stability of the catalysts was evaluated by conducting a 70 h N_2O decomposition test at 600 °C under O_2 and N_2O co-feeding conditions, simulating realistic oxidative environments Figure 1c,d. Because industrial N_2O abatement systems typically operate under oxidizing atmospheres for extended durations, such long-term O_2 durability is critical for assessing catalyst viability in commercial-scale industry.

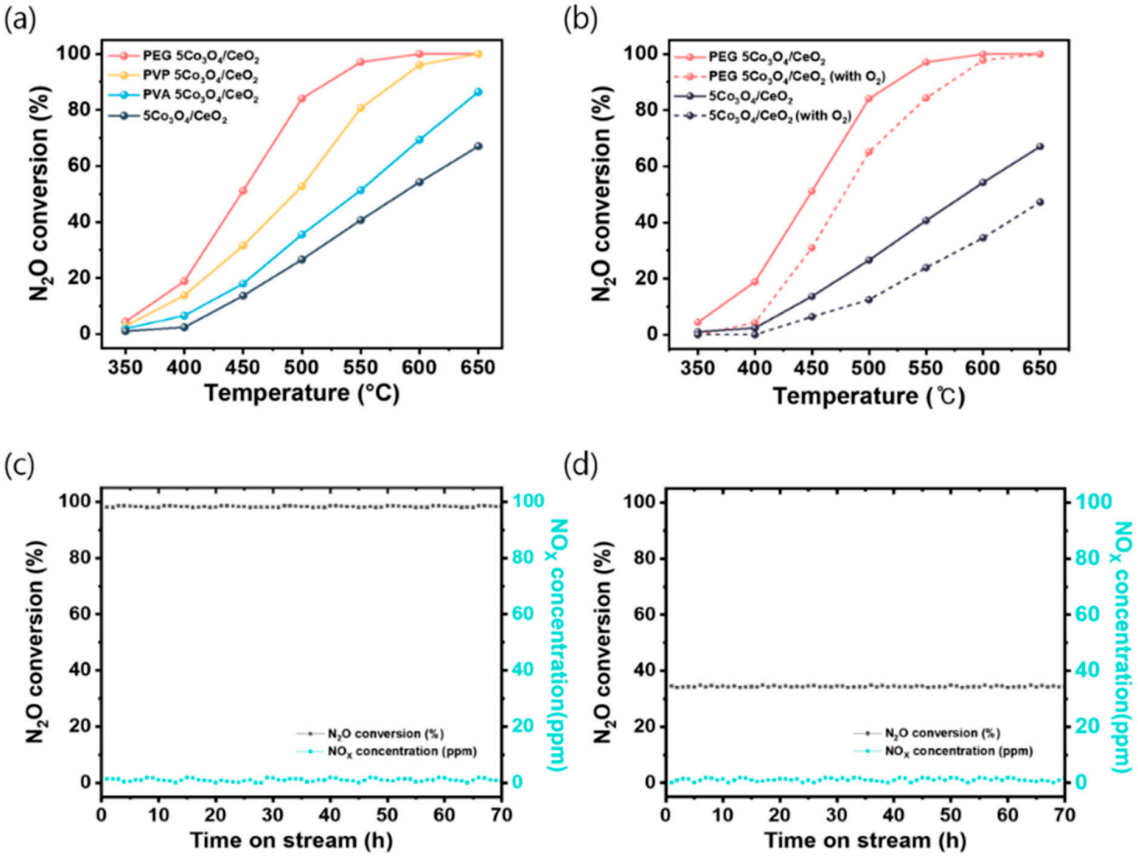

Figure 1. (**a**) N_2O decomposition activities of the PEG, PVP, and PVA-assisted $5Co_3O_4/CeO_2$ catalysts and pristine $5Co_3O_4/CeO_2$ under the following conditions: 5000 ppm N_2O, N_2 balance, GHSV of 60,000 h^{-1}, and 350–650 °C. (**b**) N_2O decomposition activities of PEG $5Co_3O_4/CeO_2$ and pristine $5Co_3O_4/CeO_2$ with and without 5 vol.% O_2 under the following conditions: 5000 ppm N_2O, N_2 balance, GHSV of 60,000 h^{-1}, and 350–650 °C. Long-term stabilities of the (**c**) PEG $5Co_3O_4/CeO_2$ and (**d**) pristine $5Co_3O_4/CeO_2$ catalysts at 600 °C for 70 h under the following conditions: 5000 ppm N_2O, 5 vol.% O_2, N_2 balance, and GHSV of 60,000 h^{-1}.

In addition, NOx concentrations in the outlet stream were monitored to assess the selectivity of the catalysts and ensure that N_2O was directly decomposed into N_2 and O_2 without proceeding through intermediate steps involving NO or NO_2 formation. Monitoring NOx is critical because N_2O can follow multiple decomposition pathways, some of which involve the formation of NO or NO_2 as intermediates [1]. These species may arise from incomplete reduction or side oxidation reactions. Their presence indicates both

a loss of selectivity toward N_2 and environmental concerns because NOx are regulated pollutants [49]. Therefore, the absence of NOx formation indicates that the reaction selectively proceeds toward N_2 and O_2 without generating harmful byproducts. Under N_2O and O_2 conditions, the PEG $5Co_3O_4/CeO_2$ catalyst exhibited only a marginal decrease in N_2O conversion (from >99.5% to 97.2%) at 600 °C. In contrast, the pristine $5Co_3O_4/CeO_2$ catalyst showed a significant reduction in performance, with the N_2O conversion decreasing from 57.6% to 35.4%. This reduction represents approximately a 20% loss in activity. Thus, the PEG additive functioned as an effective surface electronic property modulator, enhancing both redox stability and oxygen tolerance. Consequently, PEG $5Co_3O_4/CeO_2$ maintained superior catalytic activity even under oxidizing conditions.

To assess the durability of the catalysts under conditions that influence stability, time-on-stream tests were conducted at 550 and 600 °C with the stepwise introduction of O_2, NO, and H_2O into the N_2O feed stream Figure 2a. Furthermore, Figure 2b shows the N_2O decomposition of all synthesized catalysts at 600 °C under simultaneous feeding conditions. These species adversely affect catalytic performance because O_2 competes with N_2O for active sites while NO and H_2O deactivate or block surface oxygen vacancies, resulting in decreased catalytic activity [50,51]. At 550 °C, the pristine $5Co_3O_4/CeO_2$ catalyst exhibited low baseline activity (approximately 40%), which decreased more severely to 21% (with O_2), 18% (with O_2 + NO), and only 6% (with O_2 + NO + H_2O). In contrast, the PEG $5Co_3O_4/CeO_2$ catalyst initially achieved an 84% N_2O conversion under N_2O-only conditions. Upon the sequential additions of O_2, NO, and H_2O, the conversion progressively decreased to 80%, 76%, and 59%, respectively. A similar trend was observed at 600 °C. The PEG-assisted catalyst maintained >99.5% N_2O conversion under N_2O-only conditions, with only minor reductions of 97%, 95%, and 80% following co-feeding with O_2, NO, and H_2O, respectively. Conversely, the pristine catalyst started at 57% conversion and decreased to 35%, 30%, and 12% under identical conditions. These results demonstrate the superior tolerance of the PEG $5Co_3O_4/CeO_2$ catalyst to the deactivation effects of oxygen, nitrogen oxides, and water vapor, which can significantly impair the N_2O decomposition performance of conventional Co_3O_4-based catalysts. Overall, the PEG $5Co_3O_4/CeO_2$ catalyst exhibited excellent N_2O removal efficiency, enhanced resistance to common inhibitors, and stable performance under various reaction conditions. Thus, the PEG $5Co_3O_4/CeO_2$ catalyst has significant potential for practical applications in industrial emission-control systems. The CeO_2 support was excluded in the analysis to decouple the effect of polymers on cobalt.

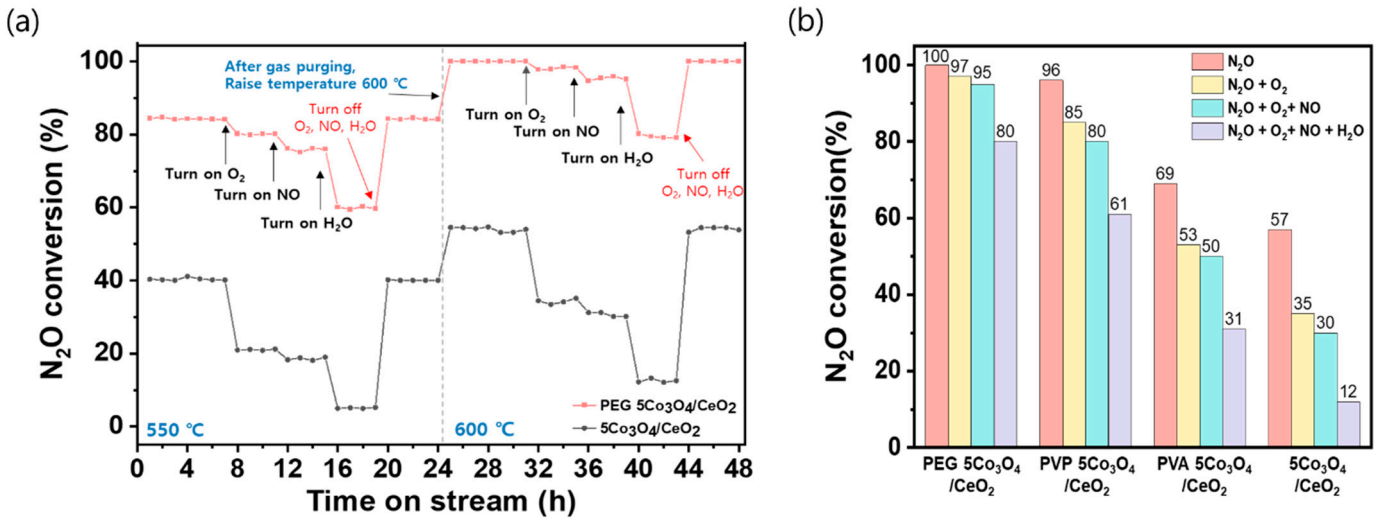

Figure 2. N_2O decomposition activities of the PEG $5Co_3O_4/CeO_2$ and pristine $5Co_3O_4/CeO_2$ catalysts under the conditions. (**a**) Time-on-stream stability test at 550 and 600 °C under sequential addition of O_2, NO, and H_2O. (**b**) All synthesized catalysts at 600 °C under simultaneous feeding O_2,

NO, and H_2O. The reaction conditions were as follows: 5000 ppm N_2O, 5 vol% O_2, 500 ppm NO, 5 vol% H_2O, N_2 balance, and GHSV of 60,000 h^{-1}.

3.2. Structural Characteristics and Surface Properties of the Catalysts

XRD was performed to examine the crystallinities and identify the crystal planes of the synthesized catalysts Figure 3a. The structure of the pristine Co_3O_4 catalyst was confirmed by characteristic peaks located at 19.1°, 31.3°, 36.8° and 44.6°, which corresponded to the (111), (220), (311), and (400) planes of Co_3O_4, respectively (JCPDS card No. 75-2480) [52]. For the polymer-assisted Co_3O_4 catalysts, a decrease in diffraction intensity was observed across all planes. In particular, the intensity of the main (311) crystal plane was significantly reduced in the PEG Co_3O_4 sample, indicating a lower crystallinity. This observation is typically associated with smaller crystallite sizes and structural disorder [53,54]. The textural properties of the catalysts were examined using BET analysis to confirm the effects of reduced crystallinity on surface properties Table 1. All polymer-assisted Co_3O_4 catalysts exhibited increased BET surface areas compared to the pristine Co_3O_4 catalyst. Among them, the PEG Co_3O_4 sample showed the highest increase in both surface area (m^2/g) and pore volume (cm^3/g). Therefore, the structural modifications induced by PEG increased the accessible surface area, which was beneficial for catalytic reactions. Based on the XRD and BET results, the reduced crystallinity and increased surface area of PEG Co_3O_4 likely enhanced the exposure of active sites, thereby improving catalytic activity for N_2O decomposition [55]. As shown in Table 1, the crystallite sizes determined using the Scherrer equation (Equation (2)) demonstrated that the PEG Co_3O_4 catalyst exhibited the smallest crystallite size among the samples. Additionally, the particle size distributions were evaluated from TEM images Figure S4, and the results indicated that the PEG Co_3O_4 catalyst exhibited smaller particle sizes compared to the pristine sample [56]. Furthermore, the SAED patterns obtained from TEM analysis confirmed the crystalline nature of the catalysts. Specifically, the pristine Co_3O_4, PVA Co_3O_4, and PVP Co_3O_4 catalysts displayed relatively sharp and distinct diffraction rings, whereas the PEG Co_3O_4 exhibited more diffuse and blurred rings, indicating a decrease in crystallinity [57,58].

$$D = \frac{K\lambda}{\beta cos\theta} \quad (2)$$

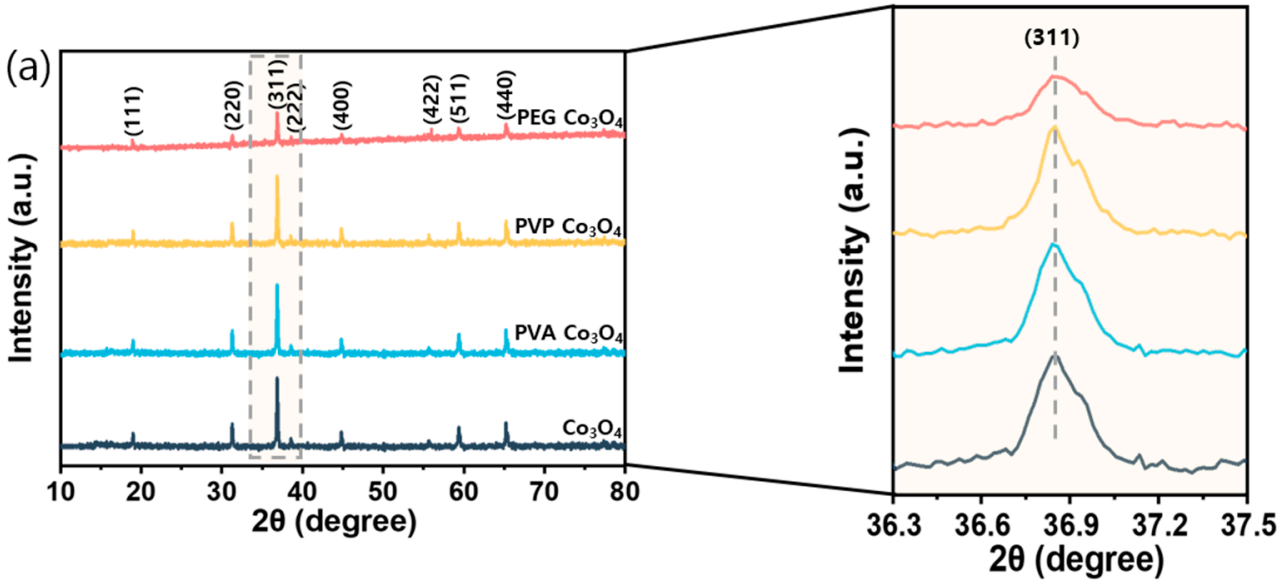

Figure 3. *Cont.*

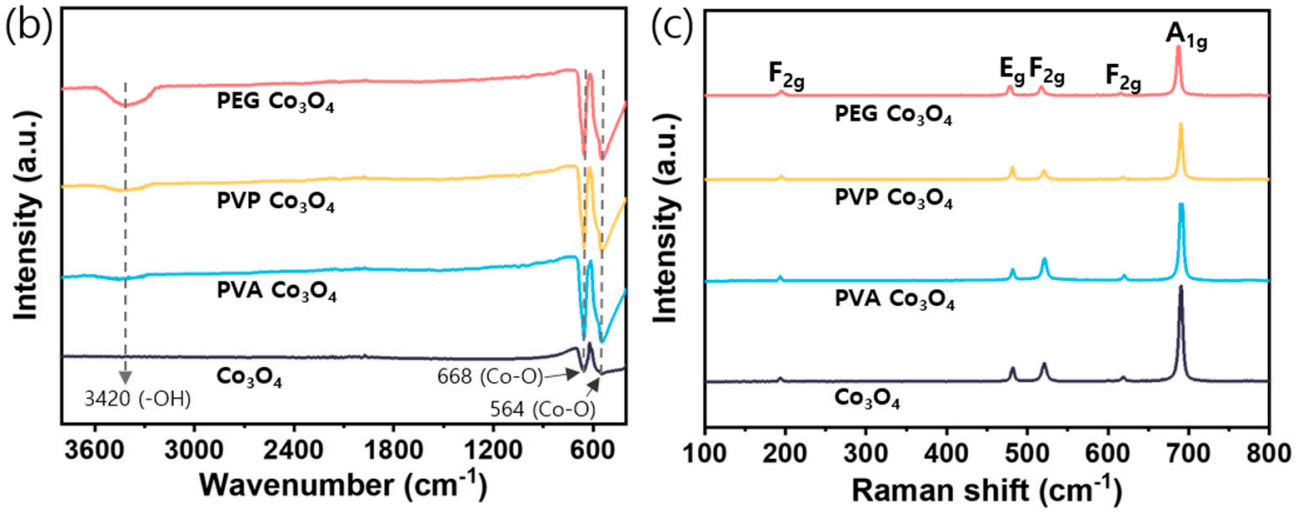

Figure 3. Structural and vibrational characterizations of PEG Co_3O_4, PVP Co_3O_4, PVA Co_3O_4, and pristine Co_3O_4 catalysts: (**a**) XRD analysis (**b**) FT-IR spectra (**c**) Raman spectra.

Table 1. BET surface areas, pore volumes and crystallite size of PEG Co_3O_4, PVP Co_3O_4, PVA Co_3O_4, and pristine Co_3O_4.

Sample	BET Surface Area (m^2/g)	Pore Volume (cm^3/g)	Pore Size (nm)	Crystallite Size (nm)
PEG Co_3O_4	35	20	17	15.64
PVP Co_3O_4	25	12	12	16.59
PVA Co_3O_4	24	12	11	16.82
Co_3O_4	18	10	10	17.25

FT-IR spectroscopy was performed to investigate the vibrational characteristics and chemical bonding of the synthesized catalysts. The FT-IR spectra of the polymer-assisted Co_3O_4 catalysts are shown in Figure 3b. These samples exhibited three characteristic absorption bands at approximately 3420, 668, and 564 cm^{-1} [59]. The broad band centered at 3420 cm^{-1} corresponded to the hydroxyl (-OH) stretching vibration. Compared to that of pristine Co_3O_4, the enhanced intensity of this hydroxyl band in the PEG Co_3O_4 sample suggests an increased surface hydroxyl content, which may be associated with higher numbers of surface defect sites and active oxygen species [60]. The presence of abundant surface hydroxyl groups can enhance catalytic activity by facilitating reactant adsorption and participating in electron transfer processes during redox reactions [61]. Two distinctive bands at 668 and 564 cm^{-1} corresponded to the Co-O stretching vibrations of Co^{2+}-O and Co^{3+}-O bonds, respectively, confirming the successful formation of a Co_3O_4 spinel structure in all synthesized catalysts [59]. When comparing the polymer-assisted catalysts with pristine Co_3O_4, significant differences were observed in the intensities of the Co_3O_4 stretching bands. For example, the polymer-assisted samples exhibited enhanced and sharper peaks at 668 and 564 cm^{-1}, suggesting improved Co_3O_4 bonding characteristics. Moreover, the increased intensity and sharpness of these characteristic peaks indicate that the polymer additives may influence the local coordination environment during Co_3O_4 formation, potentially contributing to better-defined metal–oxygen bonding in the spinel structure [40,62].

Raman spectroscopy was used to investigate the structural characteristics of the synthesized Co_3O_4 catalysts. According to group theory, spinel Co_3O_4 exhibits five Raman-active modes: A_{1g}, E_g, and three F_{2g} modes [63]. The Raman spectra of the pristine and polymer-assisted Co_3O_4 catalysts are shown in Figure 3c. All samples exhibited the three characteristic Co_3O_4 spinel bands, thus indicating the successful formation of a Co_3O_4 spinel structure without impurities. For example, the A_{1g} mode appeared at approximately

680 cm^{-1} (octahedral Co^{3+}-O_6 vibration), three F_{2g} modes were located at approximately 190, 515, and 610 cm^{-1} (tetrahedral Co^{2+}-O_4 vibrations), and the E_g mode was observed at approximately 478 cm^{-1} [50]. Notably, a gradual decrease in the A_{1g} peak intensity was observed in the polymer-assisted samples in the following order: PEG Co_3O_4 < PVP Co_3O_4 < PVA Co_3O_4 < pristine Co_3O_4. This decrease indicates a reduction from Co^{3+} to Co^{2+} during synthesis, because the A_{1g} mode is characteristic of Co^{3+} species in octahedral sites [64]. The reduction process can be attributed to the thermal decomposition of the organic polymers (PVA, PVP, and PEG), which function as mild reducing agents during calcination. Their decomposition releases carbonaceous species that facilitate the partial reduction of Co^{3+} to $Co^{2+,}$ resulting in the formation of oxygen vacancies, which play a key role in enhancing catalytic activity by providing active sites for redox reactions [64,65].

3.3. Redox Behavior and Surface Oxygen State Properties

As shown in Figure 4a and Table 2, the chemical oxidation states of cobalt were investigated using XPS. The Co 2p spectrum exhibited two primary peaks corresponding to the Co^{2+} and Co^{3+} oxidation states. Particularly, the fitted peaks near 796.4 and 781.3 eV were attributed to Co^{2+} $2p_{1/2}$ and Co^{2+} $2p_{3/2}$, respectively. Moreover, the peaks located near 794.7 and 779.6 eV were assigned to Co^{3+} $2p_{1/2}$ and Co^{3+} $2p_{3/2}$, respectively [66]. The detailed peak positions and corresponding assignments are summarized in Table S1. According to previous reports, a high number of Co^{2+} ions on the catalyst surface is advantageous for promoting N_2O decomposition because Co^{2+} can adsorb N_2O and donate electrons to weaken and cleave N-O bonds [51,67]. The Co 2p spectra revealed that the relative ratio of the Co^{2+} peaks increased in the polymer-assisted Co_3O_4 catalysts, particularly in the PEG-assisted sample, suggesting a higher surface concentration of Co^{2+} species. This increased Co^{2+} content may contribute to improved N_2O decomposition performance because Co^{2+} species serve as the primary active sites in the redox mechanism. In addition, the presence of surface oxygen species plays a crucial role in catalytic reactions. As shown in Figure 4b, the O 1s spectra of the catalysts comprised two main peaks. The peak located at 531.0–531.8 eV was attributed to surface-adsorbed oxygen species (O_{ads}), while the peak at 529.1–530.0 eV corresponded to lattice oxygen species (O_{latt}). The ratios of O_{ads}-to-O_{latt} for all samples are presented in Table 2 [44]. For the polymer-assisted Co_3O_4 catalysts, the O_{ads}/O_{latt} ratio increased depending on the type of polymer: Co_3O_4 < PVA Co_3O_4 < PVP Co_3O_4 < PEG Co_3O_4. This increase was likely due to the formation of additional oxygen vacancies induced by adding the polymer during synthesis. The enhanced formation of surface oxygen vacancies facilitated the generation of reactive oxygen species, which are beneficial for N_2O decomposition [68]. Overall, the PEG-assisted Co_3O_4 catalyst exhibited the highest $Co^{2+}/(Co^{2+} + Co^{3+})$ and $O_{ads}/(O_{ads} + O_{latt})$ ratios of 0.47 and 0.72, respectively, indicating enhanced oxygen vacancy formation and optimal surface properties for N_2O decomposition.

Table 2. XPS results of the PEG Co_3O_4, PVP Co_3O_4, PVA Co_3O_4, and pristine Co_3O_4 catalysts.

Sample	Surface Information	
	$Co^{2+}/(Co^{2+} + Co^{3+})$	$O_{ads}/(O_{ads} + O_{latt})$
PEG Co_3O_4	0.47	0.72
PVP Co_3O_4	0.43	0.64
PVA Co_3O_4	0.35	0.50
Co_3O_4	0.30	0.41

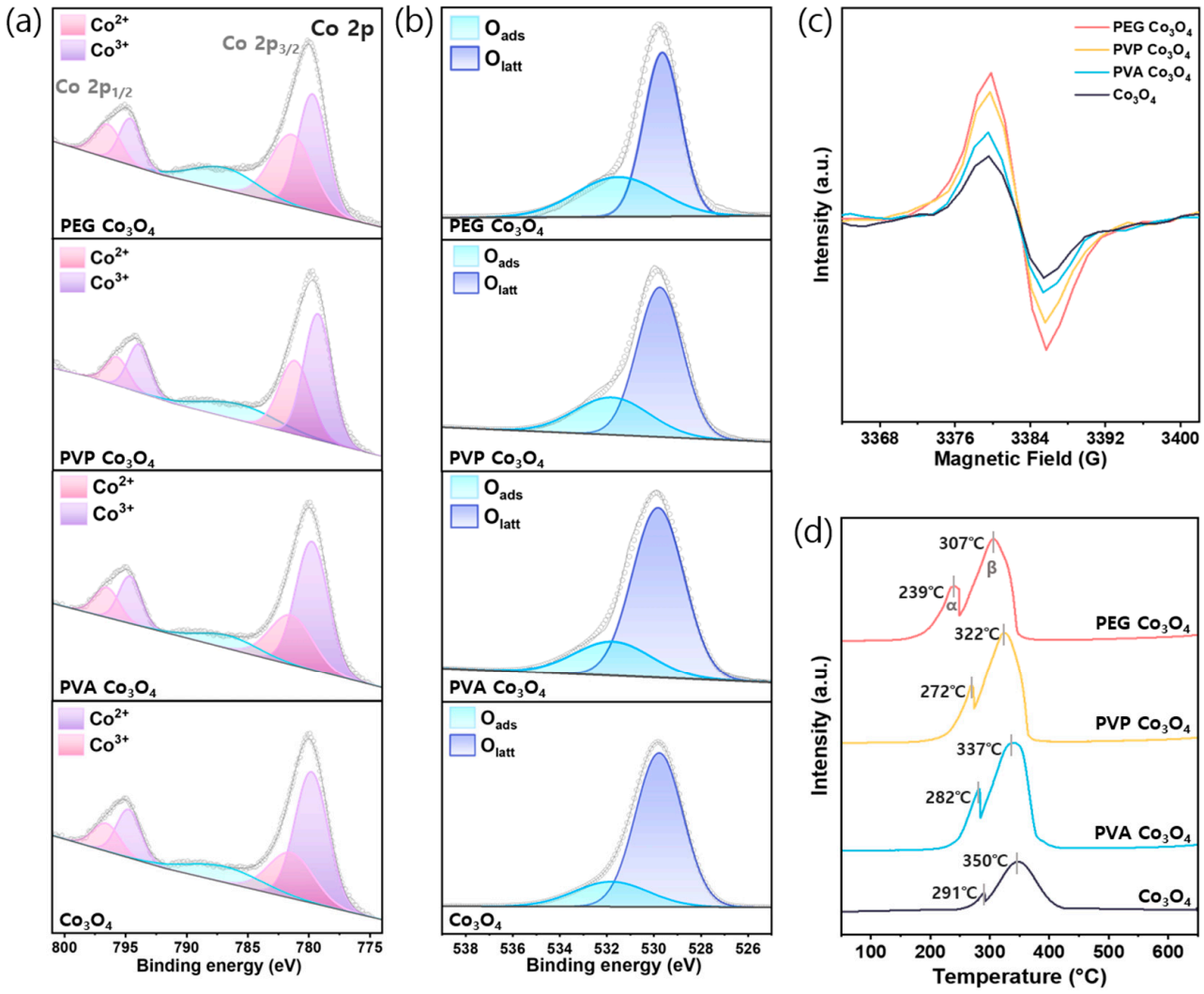

Figure 4. Surface and redox characterizations of PEG Co_3O_4, PVP Co_3O_4, PVA Co_3O_4, and pristine Co_3O_4 catalysts: (**a**) Co 2p XPS spectra (**b**) O 1s XPS spectra. (**c**) EPR spectra and (**d**) H_2-TPR profiles.

EPR spectroscopy is highly sensitive to paramagnetic species, such as unpaired electrons; thus, it was employed to investigate the presence of surface Co^{2+} species and their associated electronic states. As shown in Figure 4c, the pristine and polymer-assisted Co_3O_4 catalysts exhibited a characteristic signal at $g \approx 2.003$, corresponding to unpaired electrons localized on surface Co^{2+} ions [50]. The signal intensities followed the order: Co_3O_4 < PVA Co_3O_4 < PVP Co_3O_4 < PEG Co_3O_4, indicating an increase in the concentration of surface Co^{2+} species. It is likely that the thermal decomposition of polymer additives during calcination facilitated the formation of oxygen vacancies and promoted the generation of Co^{2+} ions on the catalyst surface. These results are consistent with the XPS analysis, further confirming the enhanced surface Co^{2+} species in the polymer-assisted Co_3O_4 catalysts [54,69].

The redox behaviors of the synthesized catalysts were investigated using H_2-TPR analysis Figure 4d. All samples exhibited two distinct hydrogen reduction peaks within the range of 50–700 °C. The first peak (denoted as α, 200–300 °C) corresponded to the reduction of Co^{3+} to Co^{2+}, while the second peak (denoted as β, 300–400 °C) corresponded to the reduction of Co^{2+} to metallic cobalt [66]. Compared to pristine Co_3O_4, both the α and β peaks of the polymer-assisted Co_3O_4 catalysts shifted to lower temperatures. Among them, the PEG-assisted Co_3O_4 catalyst exhibited the most pronounced shift, with α and

β peaks at 239 and 307 °C, respectively, indicating enhanced surface reducibility and a more facile reduction of cobalt species. These improved redox properties, particularly in PEG-assisted Co_3O_4, are expected to play a key role in enhancing catalytic performance for N_2O decomposition [44,70].

The TPD of O_2 and N_2O was performed to investigate the role of the synthesized catalysts in N_2O decomposition. First, the O_2-TPD profiles were recorded over 50–700 °C to examine the surface oxygen reactivity Figure 5a and Table S2. The total desorption amount, as shown in Figure 5b, exhibited the following trend: Co_3O_4 < PVA Co_3O_4 < PVP Co_3O_4 < PEG Co_3O_4. Notably, PEG Co_3O_4 exhibited a strong and broad desorption peak between 130 and 280 °C, attributed to active surface oxygen species [44]. Because oxygen desorption at <450 °C is generally associated with chemisorbed species (O_{ads}) [66,67], these results support the XPS findings showing elevated O_{ads}/O_{latt} ratios in the polymer-assisted samples. Therefore, the enhanced low-temperature oxygen desorption observed for PEG Co_3O_4 indicated a higher density of reactive oxygen species, which could facilitate N_2O decomposition.

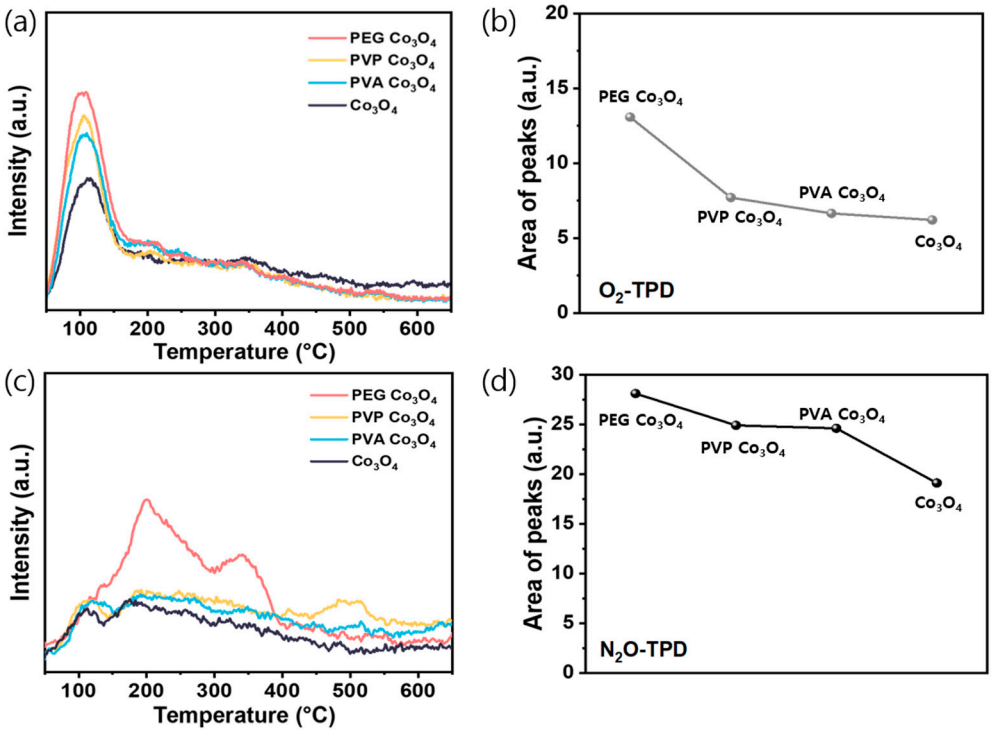

Figure 5. O_2-TPD and N_2O-TPD analyses of the PEG Co_3O_4, PVP Co_3O_4, PVA Co_3O_4, and pristine Co_3O_4 catalysts: (**a**) O_2-TPD profile (**b**) Peak areas of O_2-TPD and (**c**) N_2O-TPD profile (**d**) Peak areas of N_2O-TPD.

To evaluate the N_2O activation capacity, N_2O-TPD analysis was performed. According to previous studies, the TPD signals in this context primarily originate from the desorption of N_2O or its decomposition products adsorbed on the surface oxygen vacancies [71]. As shown in Figure 5c and Table S2, all samples displayed a primary desorption peak at <450 °C, indicating desorption of surface-adsorbed N_2O or dissociation products at vacancy sites [72]. This chemisorption-related region reflects the N_2O adsorption–dissociation capability of the catalysts. Among the samples, PEG Co_3O_4 exhibited the highest desorption intensity, followed by PVP Co_3O_4, PVA Co_3O_4, and pristine Co_3O_4. This order was confirmed by the temperature-programmed desorption curves and relative desorption peak areas shown in Figure 5a–d, highlighting that polymer addition enhanced the surface interactions and N_2O decomposition performance.

3.4. Role of Polymer

Herein, polymer-assisted metal oxide catalysts were synthesized using polymers that can regulate the particle size and morphology and induce oxygen vacancies. All polymers coordinated with cobalt precursors during nucleation, suppressing uncontrolled hydrolysis and particle aggregation, while their subsequent thermal decomposition generated reductive intermediates that partially reduced Co^{3+} to Co^{2+} and induced oxygen vacancies [31–34]. These processes collectively enhanced redox activity and surface defect density, resulting in improved catalytic performance for N_2O decomposition. Among the three polymers, PVA and PVP primarily influenced structural evolution and surface stabilization during the synthesis process. PVA, containing abundant hydroxyl groups, strongly interacted with hydrated cobalt complexes ($[Co(H_2O)_6]^{2+}$) via hydrogen bonding, forming transient core–shell structures that inhibited grain growth and promoted uniform particle dispersion. During calcination, the decomposition of PVA released mildly reducing species, such as polyene fragments, which partially reduced Co^{3+} to Co^{2+} and generated oxygen vacancies through charge compensation associated with lattice oxygen removal. This led to a higher surface Co^{2+} content and enhanced exposure of active sites [34]. PVP, in contrast, contains carbonyl and pyrrolidone nitrogen groups that coordinated with cobalt ions, mitigating excessive hydrolysis and aggregation during precursor formation. Its steric hindrance further restricted crystal growth, thereby stabilizing dispersed Co_3O_4 nanoparticles. While PVP induced fewer oxygen vacancies than PVA, it effectively maintained particle uniformity and stabilized surface Co^{2+} species by suppressing excessive oxidation during calcination [73].

In particular, PEG contributed to an increased number of surface Co^{2+} species and the formation of oxygen vacancies during the synthesis process. These features are related to structural properties and are closely associated with redox-active surface characteristics. The mechanism responsible for the increased Co^{2+} ratio during the fabrication process is presented in Figure 6 and Equations (3)–(5). After $Co(NO_3)_2{\cdot}6H_2O$ was dissolved in water to form $[Co(H_2O)_6]^{2+}$ complexes [40], the ether oxygen groups in the PEG chain were weakly coordinated to $[Co(H_2O)_6]^{2+}$. This resulted in the formation of PEG-$[Co^{2+}]$ complexes via hydrogen bonding and dipole-ion interactions. Owing to their flexible chain structure and high hydrophilicity, PEG molecules surrounded the cobalt ions, slowed hydrolysis, and facilitated uniform precipitation [74,75]. After adding NaOH, cobalt hydroxide precipitated and stabilized within the PEG matrix. During calcination, PEG decomposed particularly between 200 and 450 °C, releasing carbonaceous intermediates such as CO, CH_2O, and aldehydes. These in situ formed reducing species partially reduced Co^{3+} to Co^{2+}, while charge compensation was achieved via lattice oxygen removal, resulting in the formation of oxygen vacancies [76]. This trend is consistent with the XPS results, which showed a decreased O_{latt} signal for the PEG Co_3O_4 catalyst, indicating the generation of surface oxygen vacancies. These structural and electronic modifications hindered crystal grain growth and resulted in a higher surface area and number of redox-active sites, thereby enhancing the N_2O adsorption and activation ability of the catalyst.

$$Co(NO_3)_2{\cdot}6H_2O \rightarrow [Co(H_2O)_6]^{2+} + 2NO_3^- \quad (3)$$

$$[Co(H_2O)_6]^{2+} + 2OH^- \rightarrow Co(OH)_2 + 6H_2O \quad (4)$$

$$6Co(OH)_2 + O_2 \rightarrow 2Co_3O_4 + 6H_2O \quad (5)$$

The thermal decomposition of PEG occurred in multiple stages. First, dehydration occurred at <180 °C, followed by the degradation of hydroxyl and ether groups between 180 and 380 °C and polyether chain scission at approximately 380–500 °C. These stages released reductive fragments that interacted with the cobalt lattice during

calcination [49,76]. The resulting oxygen vacancies played a significant role in stabilizing the surface Co^{2+} species.

The Raman spectra showed a weakened A_{1g} mode associated with Co^{3+} to Co^{2+}, indicating partial reduction. The XPS Co 2p and O 1s spectra further confirmed the increased Co^{2+}/Co^{3+} and O_{ads}/O_{latt} ratios in PEG Co_3O_4. Moreover, EPR analysis revealed stronger signals at $g \approx 2.003$, indicating increased unpaired electrons from oxygen vacancies. These findings were consistent with the improved reducibility observed in the H_2-TPR results. Moreover, they were supported by the O_2-TPD and N_2O-TPD analyses, which indicated the enhanced desorption of surface oxygen species and N_2O-derived intermediates. In summary, introducing PEG during the Co_3O_4 preparation process was highly beneficial for forming catalysts with enriched surface Co^{2+} species and oxygen vacancies, thereby enhancing the catalytic performance in N_2O decomposition.

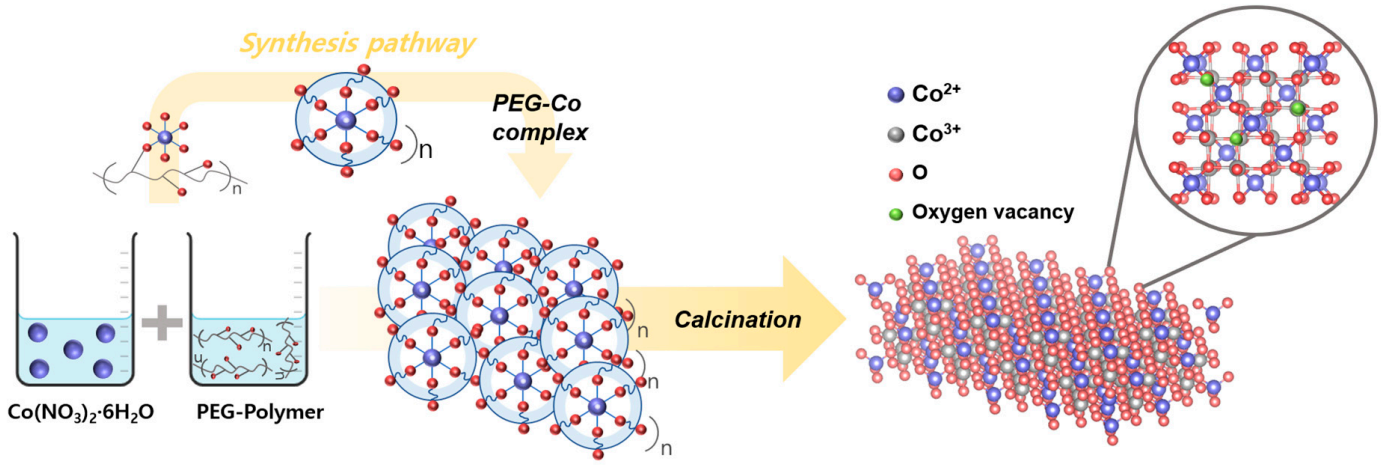

Figure 6. Synthesis pathway of the PEG Co_3O_4 catalyst, which promoted Co^{2+} formation.

4. Conclusions

An effective synthesis strategy for Co_3O_4 spinel catalysts was developed using polymer (PVA, PVP, or PEG)-assisted methods to enhance the performance of N_2O decomposition. The addition of these polymers facilitated the formation of Co^{2+}-enriched surfaces and abundant oxygen vacancies, which are primary active sites for N_2O activation. Among the polymers investigated, the PEG-assisted Co_3O_4 catalyst exhibited the most pronounced enhancement in terms of surface area, reducibility, and O_{ads}/O_{latt} ratio, as demonstrated by XRD, XPS, EPR, TPD, and H_2-TPR analyses. Notably, the unique characteristics of PEG, such as its abundant hydroxyl groups and flexible molecular chains, enabled strong interactions with cobalt precursors, thus significantly facilitating the preferential formation and stabilization of surface Co^{2+} species. The increased concentration of Co^{2+}, which is a key redox-active site in the catalytic cycle, directly contributed to superior N_2O decomposition performance. Finally, the PEG $5Co_3O_4/CeO_2$ sample achieved nearly complete N_2O conversion (>99.5%) at 600 °C. Moreover, it maintained a conversion of 97.2% under O_2 co-feeding conditions, thus outperforming catalysts synthesized without polymer additives. This study demonstrates that PEG-assisted synthesis can effectively modulate the surface chemistry of Co_3O_4 by enriching catalytically active Co^{2+} sites, thereby significantly enhancing N_2O decomposition activity. Thus, polymer-assisted spinel catalysts can be a practical approach for improving N_2O decomposition efficiency.

Supplementary Materials: The following supporting information can be downloaded at https://www.mdpi.com/article/10.3390/nano15211642/s1, Figure S1. A scheme of materials synthesis. Figure S2. N2O decomposition activity of PEG, PVP, and PVA-assisted Co_3O_4 catalysts and pristine

$5Co_3O_4$ under 5000 ppm N2O, N2 balance, GHSV 60,000 h^{-1}, in the temperature range of 350–650 °C. Figure S3. Catalytic performance and kinetic analysis of all sample catalysts for N2O decomposition. (a) N2O conversion as function of reaction temperature (b) Reaction rates at various temperature (c) Arrhenius plot (d) Activation energy (Ea). Reaction condition: 5000 ppm N2O with N2 balance, GHSV=1,000,000 h^{-1}. Figure S4. TEM images and SAED patterns of the catalysts. (a) and (b) Pristine Co_3O_4, (c) and (d) PVA Co_3O_4, (e) and (f) PVP Co_3O_4, (g) and (h) PEG Co_3O_4. Table S1. XPS peaks data of the PEG Co_3O_4, PVP Co_3O_4, PVA Co_3O_4, and pristine Co_3O_4 catalysts. Table S2. Peak area data from the O2-TPD and N2O-TPD analyses.

Author Contributions: N.K.: Conceptualization, investigation and writing (original draft). S.-J.K.: data curation and formal analysis. S.-H.S.: conceptualization. M.-J.L.: data curation and visualization. B.J.: software and methodology. H.-D.K.: supervision, project administration, and funding acquisition. T.W.N.: writing (review and editing) and validation. B.Y.: writing (review and editing), supervision, validation, and funding acquisition. All authors have read and agreed to the published version of the manuscript.

Funding: This research was financially supported by the Ministry of Trade, Industry and Energy (MOTIE) [grant number (00432416)] and the Korea Institute of Industrial Technology (KITECH-UR-24-0035 and KITECH-JA250006).

Data Availability Statement: The original contributions presented in this study are included in the article/Supplementary Material. Further inquiries can be directed to the corresponding authors.

Conflicts of Interest: The authors declare that they have no known competing financial interests or personal relationships that could have appeared to influence the work reported in this paper.

References

1. Zhuang, Z.; Guan, B.; Chen, J.; Zheng, C.; Zhou, J.; Su, T.; Chen, Y.; Zhu, C.; Hu, X.; Zhao, S.; et al. Review of nitrous oxide direct catalytic decomposition and selective catalytic reduction catalysts. *Chem. Eng. J.* **2024**, *486*, 150374. [CrossRef]
2. Wu, X.; Du, J.; Gao, Y.; Wang, H.; Zhang, C.; Zhang, R.; He, H.; Lu, G.; Wu, Z. Progress and challenges in nitrous oxide decomposition and valorization. *Chem. Soc. Rev.* **2024**, *53*, 8379–8423. [CrossRef] [PubMed]
3. Zhao, H.; Wang, P.; Li, Z.; Ao, C.; Zhao, X.; Lin, H. Improved activity and significant O_2 resistance of Cs doped Co_3O_4 catalyst for N_2O decomposition. *J. Environ. Chem. Eng.* **2024**, *12*, 113907. [CrossRef]
4. Müller, R. The impact of the rise in atmospheric nitrous oxide on stratospheric ozone. *Ambio* **2021**, *50*, 35–39. [CrossRef]
5. Li, L.; Xu, J.; Hu, J.; Han, J. Reducing Nitrous Oxide Emissions to Mitigate Climate Change and Protect the Ozone Layer. *Environ. Sci. Technol.* **2014**, *48*, 5290–5297. [CrossRef]
6. Hussain, M.; Fino, D.; Russo, N. N_2O decomposition by mesoporous silica supported Rh catalysts. *J. Hazard. Mater.* **2012**, *211–212*, 255–265. [CrossRef]
7. Xu, X.; Xu, H.; Kapteijn, F.; Moulijn, J.A. SBA-15 based catalysts in catalytic N_2O decomposition in a model tail-gas from nitric acid plants. *Appl. Catal. B Environ.* **2004**, *53*, 265–274. [CrossRef]
8. Pérez-Ramírez, J.; Kapteijn, F.; Schöffel, K.; Moulijn, J.A. Formation and control of N_2O in nitric acid production: Where do we stand today? *Appl. Catal. B Environ.* **2003**, *44*, 117–151. [CrossRef]
9. Hu, X.; Wang, Y.; Wu, R.; Zhao, L.; Wei, X.; Zhao, Y. Effects of zirconia crystal phases on the catalytic decomposition of N_2O over Co_3O_4/ZrO_2 catalysts. *Appl. Surf. Sci.* **2020**, *514*, 145892. [CrossRef]
10. You, Y.; Chang, H.; Ma, L.; Guo, L.; Qin, X.; Li, J.; Li, J. Enhancement of N2O decomposition performance by N_2O pretreatment over Ce-Co-O catalyst. *Chem. Eng. J.* **2018**, *347*, 184–192. [CrossRef]
11. Hinokuma, S.; Iwasa, T.; Kon, Y.; Taketsugu, T.; Sato, K. N_2O decomposition properties of Ru catalysts supported on various oxide materials and SnO_2. *Sci. Rep.* **2020**, *10*, 21605. [CrossRef]
12. Li, Y.; Sundermann, A.; Gerlach, O.; Low, K.-B.; Zhang, C.C.; Zheng, X.; Zhu, H.; Axnanda, S. Catalytic decomposition of N_2O on supported Rh catalysts. *Catal. Today* **2020**, *355*, 608–619. [CrossRef]
13. Richards, N.; Carter, J.H.; Nowicka, E.; Parker, L.A.; Pattisson, S.; He, Q.; Dummer, N.F.; Golunski, S.; Hutchings, G.J. Structure-sensitivity of alumina supported palladium catalysts for N_2O decomposition. *Appl. Catal. B Environ.* **2020**, *264*, 118501. [CrossRef]
14. Centi, G.; Dall'Olio, L.; Perathoner, S. Room temperature decomposition of N_2O in the presence of gaseous oxygen on prereduced Rh supported catalysts. *Catal. Lett.* **2000**, *67*, 107–112. [CrossRef]
15. Marnellos, G.E.; Efthimiadis, E.A.; Vasalos, I.A. Effect of SO_2 and H_2O on the N_2O decomposition in the presence of O_2 over Ru/Al_2O_3. *Appl. Catal. B Environ.* **2003**, *46*, 523–539. [CrossRef]

16. Zabilskiy, M.; Djinović, P.; Tchernychova, E.; Tkachenko, O.P.; Kustov, L.M.; Pintar, A. Nanoshaped CuO/CeO_2 Materials: Effect of the Exposed Ceria Surfaces on Catalytic Activity in N_2O Decomposition Reaction. *ACS Catal.* **2015**, *5*, 5357–5365. [CrossRef]
17. Pietrogiacomi, D.; Campa, M.C.; Carbone, L.R.; Tuti, S.; Occhiuzzi, M. N_2O decomposition on CoO_x, CuO_x, FeO_x or MnO_x supported on ZrO_2: The effect of zirconia doping with sulfates or K^+ on catalytic activity. *Appl. Catal. B Environ.* **2016**, *187*, 218–227. [CrossRef]
18. Galloni, M.G.; Campisi, S.; Gervasini, A.; Morandi, S.; Manzoli, M. How hydroxyapatite governs surface Cu(II) and Fe(III) structuring: Effects in the N_2O decomposition under highly oxidant atmosphere. *Appl. Catal. A Gen.* **2023**, *655*, 119101. [CrossRef]
19. Lin, F.; Andana, T.; Wu, Y.; Szanyi, J.; Wang, Y.; Gao, F. Catalytic site requirements for N_2O decomposition on Cu-, Co-, and Fe-SSZ-13 zeolites. *J. Catal.* **2021**, *401*, 70–80. [CrossRef]
20. Nobukawa, T.; Yoshida, M.; Okumura, K.; Tomishige, K.; Kunimori, K. Effect of reductants in N_2O reduction over Fe-MFI catalysts. *J. Catal.* **2005**, *229*, 374–388. [CrossRef]
21. Rutkowska, M.; Piwowarska, Z.; Micek, E.; Chmielarz, L. Hierarchical Fe-, Cu- and Co-Beta zeolites obtained by mesotemplate-free method. Part I: Synthesis and catalytic activity in N_2O decomposition. *Microporous Mesoporous Mater.* **2015**, *209*, 54–65. [CrossRef]
22. Galadima, A.; Muraza, O. Stability improvement of zeolite catalysts under hydrothermal conditions for their potential applications in biomass valorization and crude oil upgrading. *Microporous Mesoporous Mater.* **2017**, *249*, 42–54. [CrossRef]
23. Rho, Y.-J.; Yoo, Y.J.; Ryu, W.-H. Research trends on minimizing the size of noble metal catalysts for Li-CO_2 batteries: From nanoparticle to single atom. *Korean J. Chem. Eng.* **2023**, *40*, 461–472. [CrossRef]
24. Yang, W.; Wang, Q.; Dang, H.; Zhao, L.; Wu, R.; Li, J.; Wang, Y.; Zhao, Y. In-situ polymerization intercalation of montmorillonite to achieve Co_3O_4 barrier dispersion for direct catalytic decomposition of N_2O. *Appl. Catal. A Gen.* **2023**, *664*, 119329. [CrossRef]
25. Liu, H.; Yang, S.; Wang, G.; Liu, H.; Peng, Y.; Sun, C.; Li, J.; Chen, J. Strong Electronic Orbit Coupling between Cobalt and Single-Atom Praseodymium for Boosted Nitrous Oxide Decomposition on Co_3O_4 Catalyst. *Environ. Sci. Technol.* **2022**, *56*, 16325–16335. [CrossRef]
26. Gong, Y.; Liu, Z.; Li, Z.; Liu, C.; Yan, N.; Ma, L. Boosting N_2O Decomposition by Fabricating the Cs–O–Co Structure over Co_3O_4 with Single-Layer Atoms of Cs. *Environ. Sci. Technol.* **2024**, *58*, 906–914. [CrossRef]
27. Jing, Y.; He, C.; Zhang, N.; Murano, Y.; Toyoshima, R.; Kondoh, H.; Kageyama, Y.; Inomata, H.; Toyao, T.; Shimizu, K.-I. Promotional Effect of Ag on the Catalytic Decomposition of N_2O in the Presence of O_2 over the Al_2O_3-Supported Rh Catalyst. *ACS Catal.* **2023**, *13*, 12983–12993. [CrossRef]
28. Hernandez Mejia, C.; van Deelen, T.W.; de Jong, K.P. Activity enhancement of cobalt catalysts by tuning metal-support interactions. *Nat. Commun.* **2018**, *9*, 4459. [CrossRef]
29. Zhang, G.; Li, J.; Wang, Y.; Lei, L.; Zhuang, L. Controlled Aggregation of Cobalt and Platinum Atoms via Plasma Treatment for Exceptional Hydrogen Evolution Reaction Activity. *Coatings* **2024**, *14*, 1569. [CrossRef]
30. Arya, R.K.; Thapliyal, D.; Pandit, A.; Gora, S.; Banerjee, C.; Verros, G.D.; Sen, P. Polymer Coated Functional Catalysts for Industrial Applications. *Polymers* **2023**, *15*, 2009. [CrossRef] [PubMed]
31. Wu, G.; Liu, S.; Ren, J.; Zhu, J.; Yu, Y.; Yusup, S.; Chen, D.; Zhang, S.; Huang, Y. Controllable design of phosphorus-doped cobalt sulfide for catalytic conversion of cellulose to methyl levulinate: The importance of Co^{3+}/Co^{2+} ratio. *Renew. Energy* **2025**, *250*, 123322. [CrossRef]
32. Ma, Y.; Wang, L.; Ma, J.; Liu, F.; Einaga, H.; He, H. Improved and Reduced Performance of Cu- and Ni-Substituted Co_3O_4 Catalysts with Varying CoOh/CoTd and Co^{3+}/Co^{2+} Ratios for the Complete Catalytic Oxidation of VOCs. *Environ. Sci. Technol.* **2022**, *56*, 9751–9761. [CrossRef]
33. Ye, M.; Mohanty, P.; Ghosh, G. Morphology and properties of poly vinyl alcohol (PVA) scaffolds: Impact of process variables. *Mater. Sci. Eng. C* **2014**, *42*, 289–294. [CrossRef]
34. Saljoughi, E.; Mohammadi, T. Cellulose acetate (CA)/polyvinylpyrrolidone (PVP) blend asymmetric membranes: Preparation, morphology and performance. *Desalination* **2009**, *249*, 850–854. [CrossRef]
35. Masoudpanah, S.M. PVP-assisted hydrothermal synthesis of rod-like $NiCo_2O_4$ powders as high-performance microwave absorbers. *J. Mater. Res. Technol.* **2022**, *20*, 3264–3274. [CrossRef]
36. Selli, D.; Valentin, C.D. Ab Initio Investigation of Polyethylene Glycol Coating of TiO_2 Surfaces. *J. Phys. Chem. C* **2016**, *120*, 29190–29201. [CrossRef] [PubMed]
37. Do, S.-B.; Lee, S.-E.; Kim, T.-O. Oxidative decomposition with PEG-MnO_2 catalyst for removal of formaldehyde: Chemical aspects on HCHO oxidation mechanism. *Appl. Surf. Sci.* **2022**, *598*, 153773. [CrossRef]
38. Qasem Ali, A.A.; Khan, M.U.; Siddiqui, Z.N. PEG supported Cu–Mo mixed metal oxide (CuO–MoO_3@PEG): A highly efficient catalyst for the enamination of pyrimidine dione and dimedone. *Curr. Res. Green Sustain. Chem.* **2022**, *5*, 100231. [CrossRef]
39. Li, S.; Zhao, J.; Song, Z.; Wang, H.; Zhang, T.; Liu, J.; Jiang, Q. New insights into the effect of polyvinyl alcohol on Co_3O_4 spinel oxide catalyst for N_2O decomposition. *Fuel* **2024**, *362*, 130745. [CrossRef]

40. Nowakowski, L.; Hudy, C.; Zasada, F.; Gryboś, J.; Piskorz, W.; Wach, A.; Kayser, Y.; Szlachetko, J.; Sojka, Z. N_2O Decomposition on Singly and Doubly (K and Li)-Doped Co_3O_4 Nanocubes–Establishing Key Factors Governing Redox Behavior of Catalysts. *J. Am. Chem. Soc.* **2024**, *146*, 24450–24466. [CrossRef] [PubMed]
41. Bates, S.A.; Verma, A.A.; Paolucci, C.; Parekh, A.A.; Anggara, T.; Yezerets, A.; Schneider, W.F.; Miller, J.T.; Delgass, W.N.; Ribeiro, F.H. Identification of the active Cu site in standard selective catalytic reduction with ammonia on Cu-SSZ-13. *J. Catal.* **2014**, *312*, 87–97. [CrossRef]
42. Zhang, T.; Qiu, Y.; Liu, G.; Chen, J.; Peng, Y.; Liu, B.; Li, J. Nature of active Fe species and reaction mechanism over high-efficiency Fe/CHA catalysts in catalytic decomposition of N_2O. *J. Catal.* **2020**, *392*, 322–335. [CrossRef]
43. Lee, M.-J.; Jeong, B.; Kim, D.; Kim, S.-J.; Choi, Y.; Ye, B.; Kim, D.-H.; Kim, H.-D.; Cho, S. Hexagonal boron nitride heterostructure to control the oxidation states and SO_2 resistance of the V_2O_5-WO_3/TiO_2 catalyst for the NH_3-SCR reaction across a wide temperature range. *Appl. Catal. B Environ. Energy* **2025**, *378*, 125583. [CrossRef]
44. Belles, L.; Moularas, C.; Smykała, S.; Deligiannakis, Y. Flame Spray Pyrolysis Co_3O_4/CoO as Highly-Efficient Nanocatalyst for Oxygen Reduction Reaction. *Nanomaterials* **2021**, *11*, 925. [CrossRef]
45. Li, Y.; Wang, X.; Shi, C. The catalytic performance of Ba-Ce-Cu catalysts for N_2O decomposition. *J. Environ. Chem. Eng.* **2023**, *11*, 109970. [CrossRef]
46. Smeets, P.J.; Sels, B.F.; van Teeffelen, R.M.; Leeman, H.; Hensen, E.J.M.; Schoonheydt, R.A. The catalytic performance of Cu-containing zeolites in N_2O decomposition and the influence of O_2, NO and H_2O on recombination of oxygen. *J. Catal.* **2008**, *256*, 183–191. [CrossRef]
47. Grzybek, G.; Gryboś, J.; Indyka, P.; Janas, J.; Ciura, K.; Leszczyński, B.; Zasada, F.; Kotarba, A.; Sojka, Z. Evaluation of the inhibiting effect of H_2O, O_2, and NO on the performance of laboratory and pilot K-ZnxCo$_3$-xO_4 catalysts supported on α-Al_2O_3 for low-temperature N_2O decomposition. *Appl. Catal. B Environ.* **2021**, *297*, 120435. [CrossRef]
48. Yu, H.; Qi, X.; Du, X.; Pan, Y.; Feng, X.; Shan, W.; Xiong, Y. The preparation of 3.0F-Co_3O_4 catalyst with "Yardang Landform" structure and its performance for catalyzing N_2O decomposition. *Mol. Catal.* **2023**, *537*, 112960. [CrossRef]
49. Ye, B.; Jeong, B.; Lee, M.-J.; Kim, T.H.; Park, S.-S.; Jung, J.; Lee, S.; Kim, H.-D. Recent trends in vanadium-based SCR catalysts for NOx reduction in industrial applications: Stationary sources. *Nano Converg.* **2022**, *9*, 51. [CrossRef] [PubMed]
50. Li, J.-J.; Cai, S.-C.; Xu, Z.; Chen, X.; Chen, J.; Jia, H.-P.; Chen, J. Solvothermal syntheses of Bi and Zn co-doped TiO_2 with enhanced electron-hole separation and efficient photodegradation of gaseous toluene under visible-light. *J. Hazard. Mater.* **2017**, *325*, 261–270. [CrossRef]
51. Long, Y.; Zhu, X.; Gao, C.; Si, W.; Li, J.; Peng, Y. Modulation of Co spin state at Co_3O_4 crystalline-amorphous interfaces for CO oxidation and N_2O decomposition. *Nat. Commun.* **2025**, *16*, 1048. [CrossRef]
52. Wójcik, S.; Grzybek, G.; Stelmachowski, P.; Sojka, Z.; Kotarba, A. Bulk, Surface and Interface Promotion of Co_3O_4 for the Low-Temperature N_2O Decomposition Catalysis. *Catalysts* **2020**, *10*, 41. [CrossRef]
53. Makhlouf, S.A.; Bakr, Z.H.; Aly, K.I.; Moustafa, M.S. Structural, electrical and optical properties of Co_3O_4 nanoparticles. *Superlattices Microstruct.* **2013**, *64*, 107–117. [CrossRef]
54. St-Onge, V.; Cui, M.; Rochon, S.; Daigle, J.-C.; Claverie, J.P. Reducing crystallinity in solid polymer electrolytes for lithium-metal batteries via statistical copolymerization. *Commun. Mater.* **2021**, *2*, 83. [CrossRef]
55. Zhou, X.J.; Shi, P.H.; Qin, Y.F.; Fan, J.C.; Min, Y.L.; Yao, W.F. Synthesis of Co_3O_4/graphene composite catalysts through CTAB-assisted method for Orange II degradation by activation of peroxymonosulfate. *J. Mater. Sci. Mater. Electron.* **2016**, *27*, 1020–1030. [CrossRef]
56. Yu, H.; Li, Y.; Pan, Y.; Du, Y.; Feng, X.; Cui, J.; Lou, Z.; Shan, W.; Xiong, Y. Dy and K double-additive modified Co_3O_4 catalyst with high resistance to NOx for catalyzing N_2O decomposition. *Chem. Eng. J.* **2025**, *504*, 159032. [CrossRef]
57. Uvarov, V.; Popov, I. Metrological characterization of X-Ray diffraction methods for determination of crystallite size in nano-scale materials. *Mater. Charact.* **2007**, *58*, 883–891. [CrossRef]
58. Kenyota, N.; Jarernboon, W.; Laokul, P. Bulk synthesis of chemically activated carbon and cobalt oxide nanocomposites as supercapacitor electrodes. *J. Mater. Sci. Mater. Electron.* **2024**, *35*, 158. [CrossRef]
59. Rokicińska, A.; Łątka, P.; Olszański, B.; Żurowska, M.; Dębosz, M.; Michalik, M.; Kuśtrowski, P. Polymer template assisted construction of spherical Co_3O_4@meso-SiO_2 yolk-shell nanoreactors for catalytic combustion of volatile organic compounds. *Chem. Eng. J.* **2024**, *480*, 148173. [CrossRef]
60. Ercolino, G.; Grodzka, A.; Grzybek, G.; Stelmachowski, P.; Specchia, S.; Kotarba, A. The Effect of the Preparation Method of Pd-Doped Cobalt Spinel on the Catalytic Activity in Methane Oxidation Under Lean Fuel Conditions. *Top. Catal.* **2017**, *60*, 333–341. [CrossRef]
61. Wang, Y.; Wei, X.; Hu, X.; Zhou, W.; Zhao, Y. Effect of Formic Acid Treatment on the Structure and Catalytic Activity of Co_3O_4 for N2O Decomposition. *Catal. Lett.* **2019**, *149*, 1026–1036. [CrossRef]
62. Jiang, Z.; Feng, X.; Deng, J.; He, C.; Douthwaite, M.; Yu, Y.; Liu, J.; Hao, Z.; Zhao, Z. Atomic-Scale Insights into the Low-Temperature Oxidation of Methanol over a Single-Atom Pt1-Co_3O_4 Catalyst. *Adv. Funct. Mater.* **2019**, *29*, 1902041. [CrossRef]

63. Kang, B.; Guo, M.; Wu, H.; Guo, X.; Di, Z.; Wei, Y.; Jia, J.; Wang, Z.-J.; Zhang, R. Effect of alkali/alkaline-earth-metal doping on the Co_3O_4 spinel structure and N 2 O decomposition. *Catal. Sci. Technol.* **2024**, *14*, 2825–2837. [CrossRef]
64. Xue, L.; Zhang, C.; He, H.; Teraoka, Y. Catalytic decomposition of N_2O over CeO_2 promoted Co_3O_4 spinel catalyst. *Appl. Catal. B Environ.* **2007**, *75*, 167–174. [CrossRef]
65. Asano, K.; Ohnishi, C.; Iwamoto, S.; Shioya, Y.; Inoue, M. Potassium-doped Co_3O_4 catalyst for direct decomposition of N_2O. *Appl. Catal. B Environ.* **2008**, *78*, 242–249. [CrossRef]
66. Yi, S.; Lai, P.; Ma, G.; Pan, J.; Chen, Z.; Qin, Y.; Jiang, X. Green and facile synthesis of nanostructured Co_3O_4/CeO_2 catalysts via a glucose-urea method for NO oxidation. *Appl. Surf. Sci.* **2023**, *626*, 157180. [CrossRef]
67. Zhang, L.; Jin, Z.; Tsubaki, N. Zeolitic Imidazolate Framework-67-Derived P-Doped Hollow Porous Co_3O_4 as a Photocatalyst for Hydrogen Production from Water. *ACS Appl. Mater. Interfaces* **2021**, *13*, 50996–51007. [CrossRef]
68. Chen, X.; Li, J.; Cai, S.; Chen, J.; Jia, H. Two-step pyrolytic engineering of carbon-doped Co_3O_4 with rich defects for efficient low-temperature CO oxidation. *J. Mater. Chem. A* **2020**, *8*, 6619–6630. [CrossRef]
69. Wang, Z.; Wang, W.; Zhang, L.; Jiang, D. Surface oxygen vacancies on Co_3O_4 mediated catalytic formaldehyde oxidation at room temperature. *Catal. Sci. Technol.* **2016**, *6*, 3845–3853. [CrossRef]
70. Wang, Q.; Yang, W.; Dang, H.; Li, L.; Wu, R.; Wang, Y.; Zhao, Y. Enhancement of N_2O decomposition performance by co-doping of Ni and Y to Co_3O_4 catalyst. *J. Environ. Chem. Eng.* **2024**, *12*, 112463. [CrossRef]
71. Zhao, F.; Wang, D.; Li, X.; Yin, Y.; Wang, C.; Qiu, L.; Yu, J.; Chang, H. Enhancement of Cs on Co_3O_4 for N_2O Catalytic Decomposition: N_2O Activation and O_2 Desorption. *Ind. Eng. Chem. Res.* **2022**, *61*, 13854–13862. [CrossRef]
72. Shirayama, S.; Uda, T. Recovery of Cobalt Ion into Polyethyleneglycol (PEG) Gel Phase as Thiocyanato Complex. *Mater. Trans.* **2015**, *56*, 610–616. [CrossRef]
73. Yoo, S.H.; Kim, J.H.; Jho, J.Y.; Won, J.; Kang, Y.S. Influence of the addition of PVP on the morphology of asymmetric polyimide phase inversion membranes: Effect of PVP molecular weight. *J. Membr. Sci.* **2004**, *236*, 203–207. [CrossRef]
74. Ma, S.; Bai, J.; Sun, L.; Zhao, L.; Tan, H.; Liu, L.; Peng, Z.; Zhao, X.; Xiong, D. Investigation of polyethylene glycol (PEG) assisted solvothermal synthesis of $CuCoO_2$ nanosheets for efficient oxygen evolution reaction. *Dalton Trans.* **2023**, *52*, 13750–13757. [CrossRef] [PubMed]
75. Han, S.; Kim, C.; Kwon, D. Thermal degradation of poly(ethyleneglycol). *Polym. Degrad. Stab.* **1995**, *47*, 203–208. [CrossRef]
76. Krause, B.; Pötschke, P. Polyethylene Glycol as Additive to Achieve N-Conductive Melt-Mixed Polymer/Carbon Nanotube Composites for Thermoelectric Application. *Nanomaterials* **2022**, *12*, 3812. [CrossRef]

Disclaimer/Publisher's Note: The statements, opinions and data contained in all publications are solely those of the individual author(s) and contributor(s) and not of MDPI and/or the editor(s). MDPI and/or the editor(s) disclaim responsibility for any injury to people or property resulting from any ideas, methods, instructions or products referred to in the content.